ISSN 1 746-7233, England, UK
World Journal of Modelling and Simulation
Vol. 8 (2012) No. 2, pp. 83-95

Hydromagnetic viscous flow in a rotating annular high-porosity medium with nonliner forchheimer drag effects: numerical study

Osman Anwar Bêg[1], * Oluwole Daniel Makinde[2], Joaquin Zueco and Swapan[3], Swapan Kumar Ghosh[4]

[1] Aerospace Engineering, Department of Engineering and Mathematics, Sheaf Building, Sheffield Hallam University, Sheffield S11WB, U. K.
[2] Faculty of Engineering, Cape Peninsula University of Technology, Bellville 7535-1906, South Africa
[3] Thermal Engineering, ETS Ingenieros Industriales Campus Muralla del Mar, Departamento de Ingenierła Térmicay Fluidos, Universidad Politécnica de Cartagena, Cartagena (Murcia) 30203, Spain
[4] Magnetohydrodynamics Research Program, Applied Mathematics Section, Department of Mathematics, Narajole Raj College, West Bengal 721-211, India

(*Received February 1 2011, Accepted January 1 2012*)

Abstract. A mathematical model is presented for the steady, axisymmetric, magnetohydrodynamic (MHD) flow of a viscous, Newtonian, incompressible, electrically-conducting liquid in a highly porous regime intercalated between two concentric rotating cylinders in the presence of a radial magnetic field. The porous medium is modeled using a Darcy-Forchheimer drag force approach to simulate the impedance effects of the porous medium fibers at both low velocities and also at higher velocities. The tangential and axial momentum equations are non-dimensionalized with the Nath transformations [33] and rendered into a system of nonlinear, second order, second degree partial differential conservation equations subject to appropriate non-slip boundary conditions. Solutions are obtained using both the MAPLE Library finite difference algorithm and the Network Simulation Method. The influence of Hartmann number (Ha), rotational Reynolds number (Re_R), Darcy number (Da), Forchheimer number (Fs), pressure gradient parameter (α) and cylinder relative rotation rate (N) on the dimensionless tangential (U_e) and axial (U_Z) velocity components is studied in detail for the case where the cylinder walls are insulated. Excellent agreement is achieved between both methods. Applications of this study include hybrid porous media MHD power generators, magnetic materials processing and chemical engineering.

Keywords: magnetohydrodynamics, rotation, nonlinear porous media, chemical engineering, network simulation numerical method, MAPLE

1 Introduction

Viscous magnetohydrodynamic (MHD) flows arise in many applications in energy systems, chemical technology, astrophysics and flow control processes in the mechanical engineering industry. Numerous flow scenarios have been studied both analytically and with numerical analyses, including channel flows, rotating flows, spinning disk flows, annular flows between concentric cylinders, revolving pipe flows etc. Rotational effects are significant in MHD rotating generators, geophysical flows incorporating the earth's Coriolis effect and also astrophysical plasma-dynamics. Hughes and Elco [25] studied hydromagnetic tribological flow between rotating parallel disks for an axial magnetic field with a radial current and a radial magnetic field with an axial current, showing that the frictional torque on the rotor vanishes for both field configurations with the provision of electrical energy via electrodes to the fluid. Katukani [24] further investigated the magnetohydrodynamic flow from a spinning single disk. Kumar [27] investigated the steady state MHD flow in an annulus with radial magnetic field present. Other studies include those by Vidyanidhi and Rao [48] and

* Corresponding author. *E-mail address*: O.Beg@shu.ac.uk.

Stephenson [44], the latter using numerical, asymptotic and experimental methods. Nath [33] presented exact solutions for the hydromagnetic Navier-Stokes equations in steady axisymmetric flow viscous flow between two concentric rotating cylinders composed of an insulating material under the influence of radial magnetic field, showing that magnetic field strongly retards the flow and causes the tangential velocity to become fully developed in a smaller axial distance than in the absence of the magnetic field. This study also showed that for low Reynolds numbers, the fully developed tangential velocity is attained in a small axial distance, with the converse apparent for large Reynolds numbers. Lin [29] also investigated the MHD viscous flow in the annular region between between concentric rotating cylinders. Arora and Gupta [3] derived exact solutions for the magnetohydrodynamic flow between two rotating coaxial (insulator) cylinders under a radial magnetic field. Mahapatra [30] studied the viscous hydromagnetic flow through two porous non-conducting infinite circular cylinders rotating with various angular velocities for some time in the presence of a radial magnetic field, assuming that the rate of suction at the inner cylinder and the rate of injection at the outer cylinder are equal and neglecting induced electric and magnetic field effects. Sengupta and Ghosh [39] investigated a similar problem to that reported in [30]. Pop [34] considered impulsive effects in the magnetohydrodynamic viscous flow from a spinning disk. Debnath [15] has considered periodic flow effects in rotating MHD boundary layers using asymptotic analysis. Sastry and Rao [38] studied the magneto-hydrodynamic Stokes flow past a rotating sphere with the external magnetic field generated by a magnetic pole placed at the centre of the sphere, using both perturbation and computational techniques, showing that the flow reversal (due to rotation) at the rear regime of the sphere is boosted with magnetic field. Prasad and Rao [35] have investigated the MHD flow between two parallel porous walls under a constant pressure gradient rotating about an axis perpendicular to the walls, showing that the regime is dictated by the Taylor number, pressure gradient, suction Reynolds number and the Hartmann number and that when Taylor number approaches infinity, thin boundary layers are generated near the porous walls and an increase in Hartmann number (i.e. magnetic field) reduces boundary layer thickness. Debnath et al. [16] considered the effect of Hall currents on transient MHD rotating flow from a plate with surface transpiration. Seth et al. [41] considered the asymptotic behaviour of transient rotating MHD Couette-Hartmann flow (for both an impulsive start as well as accelerated start of one moving plate) at small and large time, showing that shear stress components due to the primary flow decrease, whereas those associated with the secondary flow increase with the intensity of rotation. Seth and Ghosh [40] considered the effect of oscillating pressure gradient on transient MHD flow in a rotating channel with inclined magnetic field, showing using asymptotic analysis that for high values of Hartmann number, inverse Ekman number and frequency that the flow regime is delineated into two zones, namely the boundary layer region and the central core region, and that backflow is caused in the direction of the pressure gradient for large values of inverse Ekman number (strong rotation and weak Coriolis force) and frequency for certain thresholds of the frequency. Hamza [21] studied numerically the hydromagnetic squeezing film flow between two rotating parallel plane surfaces with transverse magnetic field. Singh et al. [43] analyzed numerically the hydromagnetic flow in the annular zone between a coaxial rotating cone and a cylinder with radial magnetic field. Leeorin et al. [28] obtained linear solutions for the axisymmetric hydromagnetic flow between differentially rotating spheres permeated by an axisymmetric potential magnetic field with dipole parity with the regions external to the shell being rigid insulators and slow steady axisymmetric motion driven by rotating the inner sphere at a slightly slower rate. Meena and Kandaswamy [31] discussed steady two dimensional hydromagnetic viscous flow between two rotating eccentric cylinders with radial magnetic field as a model of a journal bearing, showing that increasing magnetic field enhances the load carrying capacity of the journal bearing. These studies have all been confined to regimes of pure fluids. In extensive technological applications the regime may contain a porous medium. Magnetohydrodynamic flows in porous media have stimulated considerable attention owing to the importance of such flows in magnetic materials processing[20], chemical engineering[32] and geophysical energy systems[47]. Ghosh and Ghosh [19] studied hydromagnetic dusty viscoelastic flow in a Darcian porous regime. Geindreau and Auriault [18] derived the tensorial filtration law in rigid porous media for steady-state slow magnetohydrodynamic viscous Newtonian flow, deriving the seepage law under a magnetic field by upscaling the flow at the pore scale. Implementing multiple-scale expansions for finite Hartmann number they showed that the macroscopic mass flow and electric current are coupled and both functions of the macroscopic gradient of pressure and the electric field and also showed that the filtration law is an

extended for of Darcy's law with a supplementary term proportional to the electric field and that the permeability tensor, which strongly depends Hartmann number. Bég et al. [7] studied the hydromagnetic oscillating heat transfer in a Darcian regime with heat generation/absorption using a perturbation technique. Hayat et al. [22] studied a variety of magnetohydrodynamic flows of a non-Newtonian fluid in a porous medium using a modified Darcy's law with Hall current effects, presenting closed-form solutions for velocity distribution valid at large and small times. Hayat et al. [23] also studied magnetohydrodynamic Jeffery non-Newtonian fluid flow in a two-dimensional porous medium channel with compliant walls with sinusoidal traveling waves on the channel walls again using a Darcy model. Khan et al. [26] employed the homotopy method to derive analytical solutions for the magnetohydrodynamic flow of Sisko rheological fluid a porous medium also using the modified Darcy's law. These studies were confined to low-velocity regimes wherein the Darcian model is valid. At higher Reynolds numbers (in excess of 10), Bear [17] and Dybbs and Edwards [4] have shown that inertial effects become important and the Darcy model must be extended to simulate such drag effects. The Forchheimer quadratic porous drag model is a simple but accurate mechanism for analyzing such flows, in particular within the context of viscous hydrodynamics. The authors have implemented the Darcy-Forchheimer (D-F) drag force model recently in many diverse fluid dynamics studies. Bhargava et al. [12] studied the pulsating rheological flow in a D-F porous medium conduit using finite elements. Takhar et al. [46] studied the viscoelastic flow with wall transpiration in a saturated D-F porous regime. More recently Bég et al. [6] extended the model in [46] to also consider heat transfer effects. In the context of magnetohydrodynamic porous flows, the D-F model (and its extensions) has also received some attention. Takhar and Bég et al. [45] used a finite difference numerical method to study hydromagnetic free convection in a porous regime. Chamkha [13] studied the Hall current effects on Darcy-Forchheimer natural MHD convection flow in a porous medium with thermal stratification effects. Bhargava et al. [11] analyzed the hydromagnetic pulsating flow with species dispersion in a two-dimensional channel containing a D-F porous material with applications in blood flow. Other recent studies include the articles by Rawat et al. [37] and more recently by Bég et al. [5] the latter presenting the first solutions in the literature relating to biomagnetic-micropolar flow and thermal convection in a D-F porous regime. Magnetohydrodynamic convection flow in rotating porous media is also of interest in chemical engineering flow processes. Recently Prasad et al. [36] obtained network numerical solutions for the effect of Ekman number and magnetic field inclination on magnetohydrodynamic flow in a rotating non-Darcian porous medium channel with Hall current effects. Sharma et al. [42] studied analytically the hydromagnetic forced flow through a Darcian porous medium adjacent to a spinning disk.

In the present study we shall extend the seminal work of Nath [33] to consider both analytically and numerically the effect of Darcian and Forchheimer drag forces on the axial fully developed MHD flow in the annular regime between two concentric rotating cylinders under a radial magnetic field. Such a study has to the authors' knowledge not appeared in the scientific communications thusfar and is an interesting addition to the existing body of knowledge. Both network numerical thermodynamic and MAPLE finite difference methods are used achieving excellent agreement.

2 Mathematical model

Let us consider the Newtonian, steady, incompressible, electrically-conducting viscous axial MHD flow between two concentric cylinders composed of insulating material and containing an isotropic, homogenous porous material saturated with the fluid, in an (r, θ, z) coordinate system. Magnetic Reynolds number is assumed to be small so that magnetic induction effects can be ignored. Also the applied radial magnetic field is weak enough to neglect Hall current and ionslip current effects. No separation of charges occurs and the body surface is not charged so that electrical field everywhere vanishes i.e. $E = 0$. An axial pressure gradient is applied and the cylinders are rotated at velocities which are lower than the threshold required to initiate Taylor vortices. The physical regime is illustrated in Fig. 1 below. As shown by Nath [33] the tangential velocity profile produced in a viscous fluid by the rotating cylinders (in the absence of Taylor vortex motions) becomes a function of the axial coordinate when an axial velocity is superimposed, irrespective of whether fully developed flow has been attained or not. For an annulus of sufficient extent, the tangential profile will approach the fully developed state when it becomes independent of axial position. The two cylinders The radial

magnetic field, B_r is generated by passing a steady electric current parallel to the axis of the coaxial cylinders, where the cylinders terminate at perfect electrodes which are connected via a load. As indicated by Nath [33], an alternative technique to achieve the desired magnetic field is through the implementation of a permeable core within the annulus and a permeable cylinder shell outside the annulus. As such the magnetic flux lines would close via these permeable paths at significant distances from the regime of interest. The "source" of the magnetic flux would be discs of permanently magnetized material between the paths and the annulus channel.

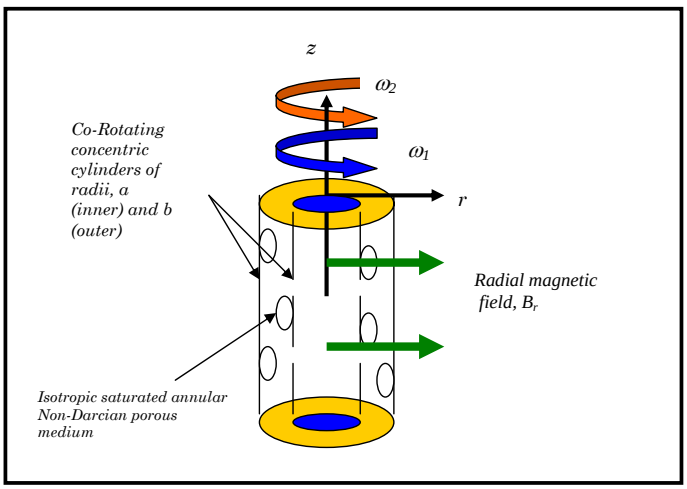

Fig. 1. Physical model and coordinate system

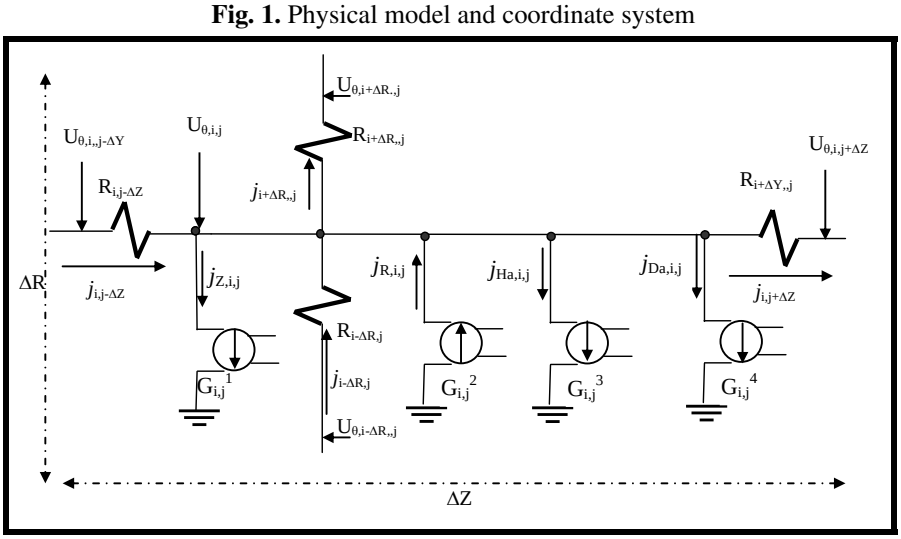

Fig. 2. Network model for tangential momentum Eq. (10)

Following Nath [33] and implementing the Darcy-Forchheimer drag force model, following Bég et al. [5], the Navier-Stokes equations in cylindrical coordinates for the magnetohydrodynamic saturated porous regime can be shown to reduce to the following form:

$$\frac{\rho u_\theta^2}{r} = \frac{\partial p}{\partial r}, \tag{1}$$

$$u_\theta \frac{\partial u_\theta}{\partial z} = \nu \left[\frac{\partial^2 u_\theta}{\partial r^2} + \frac{1}{r}\frac{\partial u_\theta}{\partial r} - \frac{u_\theta^2}{r^2} + \frac{\partial^2 u_\theta}{\partial z^2} \right] - \frac{\sigma u_\theta B_r^2}{\rho} - \frac{\nu u_\theta}{K} - \frac{\Gamma u_\theta^2}{K}, \tag{2}$$

$$\frac{1}{\rho}\frac{\partial p}{\partial z} = \nu\left[\frac{\partial^2 u_z}{\partial r^2} + \frac{1}{r}\frac{\partial u_z}{\partial r}\right] - \frac{\sigma u_z B_r^2}{\rho} - \frac{\nu u_z}{K} - \frac{\Gamma u_z^2}{K}, \tag{3}$$

$$\frac{\partial}{\partial r}(rB_r) = 0, \tag{4}$$

in which u_θ, u_z are the tangential and axial velocity components, respectively, ρ is hydrostatic pressure, ρ is fluid density, σ is fluid electrical conductivity, ν is fluid kinematic viscosity, K is the porous medium permeability (isotropic i.e. the same in $r-$and $z-$directions) and Γ is the Forchheimer geometric inertial drag parameter. Following Nath [33], Eq. (4) implies that the radial magnetic field component, B_r is proportional to $\frac{1}{r}$. Since at $r = a$ (inner cylinder radius), $B_r = A/a$, therefore $B_r = A/r$. To generate solutions independent of the dimensions of the regime, we introduce the following non-dimensional variables:

$$\begin{aligned}
&P = \left(\frac{p}{0.5\rho\omega_2^2 b^2}\right), \quad U_\theta = \frac{u_\theta}{\omega_2 b}, \quad U_z = \frac{u_z}{\omega_2 b}, \quad R = \frac{r}{b},\\
&Z = \frac{z}{b}, \quad \beta = \frac{B_r}{B_0} = \frac{1}{R}, \quad Ha^2 = \frac{\sigma B_0^2 b^2}{\mu}, \quad Re = \frac{\omega_2 b^2}{\nu}\nu,\\
&Re\frac{\partial P}{\partial Z} = -\alpha(\alpha > 0), \quad \lambda = \frac{a}{b}, \quad Da = \frac{K}{b^2}, \quad Fs = \frac{\Gamma}{b},
\end{aligned} \tag{5}$$

in which P is dimensionless pressure, U_e is dimensionless tangential velocity, U_z is dimensionless axial velocity, R is the dimensionless radial coordinate, Z is dimensionless axial coordinate, β is the magnetic field ratio, B_0 is the characteristic magnetic induction, Ha is Hartmann number, Re is rotational Reynolds number, $\frac{\partial P}{\partial Z}$ is dimensionless axial pressure gradient (to be prescribed), λ is the cylinder radius ratio (outer: inner), Da is the Darcy number and Fs is the Forchheimer number. Implementing Eq. (5) in Eqs. (1) $\sim$ (4) we obtain the following dimensionless equations:

$$\frac{\partial P}{\partial R} = \frac{1}{2}\frac{U_\theta^2}{R}, \tag{6}$$

$$R_e U_z\frac{\partial U_\theta}{\partial Z} - \frac{\partial^2 U_\theta}{\partial Z^2} = \frac{\partial^2 U_\theta}{\partial R^2} + \frac{1}{R}\frac{\partial U_\theta}{\partial R} - (1+Ha^2)\frac{U_\theta}{R^2} - \frac{U_\theta}{Da} - \frac{FsReU_\theta^2}{Da}, \tag{7}$$

$$\frac{\partial^2 U_z}{\partial R^2} + \frac{1}{R}\frac{\partial U_z}{\partial R} - \frac{Ha^2}{R^2}U_z - \frac{U_z}{Da} - \frac{FsReU_z^2}{Da} = -\alpha. \tag{8}$$

The appropriate boundary conditions are:

$$\begin{cases} U_\theta(R,0) = 0 & U_\theta(1,Z) = 1\\ U_\theta(\lambda,Z) = \frac{\omega_1 a}{\omega_2 b} = N & U_e(R,\infty) = 1\\ U_z(1) = 0 & U_z(\lambda) = 0 \end{cases} \tag{9}$$

3 Finite difference solutions with maple software library

Eqs. (6) $\sim$ (8) are nonlinear second order partial differential equation and are solved numerically using finite difference method implemented in MAPLE [1]. In these computations, the following default values were prescribed: $Ha^2 = 5$, $N = 0.4$, $R_e = 10$, $Fs = 1$, $Da = 1$, $\lambda = 0.5$, $\alpha = 1$. Such values correspond to a highly permeable regime under low magnetic field so that Hall and ionslip current effects are not mobilized in the electrically-conducting fluid. We are primarily concerned with the radial spatial distributions of velocity profiles in the regime. λ is defined as radius of inner to outer cylinder, maintained at 0.5 throughout the computations. $\alpha = 1$ corresponds to a constant axial pressure gradient of unity. Here we dwell on the influence of Ha^2, N, Da, Fs and α on U_Z and U_θ. Shear stress profiles may also be derived from these velocities although for brevity they are omitted in the present study.

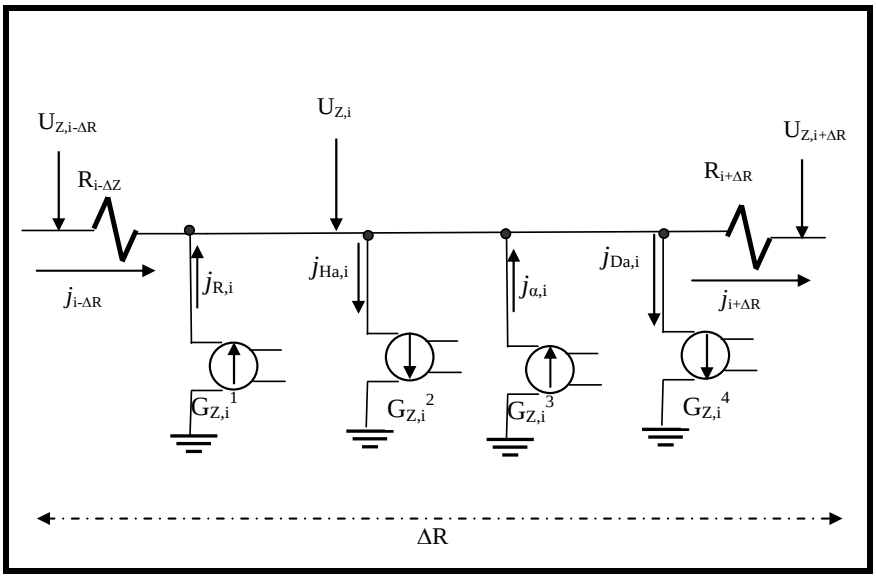

Fig. 3. Network model for axial momentum Eq. (11)

4 Networks simulation method solutions

The set of Eqs. (6) $\sim$ (8) with conditions Eq. (9) are also solved using the Network Simulation Model (NSM). Discretization of the set equations is based on the finite-difference formulation. It is assumed that the electrical variable of voltage is equivalent to for example the velocity, while the current is equivalent to the velocity flux. A network electrical model for each volume element is designed, in such a way that its electrical equations are formally equivalent to the spatial discretized equation. The whole network model, including the devices associated with the boundary conditions, is solved by the numerical computer code Pspice [2, 49]. NSM has been successfully implemented in recent years to a diverse spectrum of magneto-hydrodynamic flows. Bég et al. [9] used NSM to analyze the thermal convection in a stratified porous regime. Bég et al. [8] have also investigated hydromagnetic free convection from a spherical body in a porous regime, rotating magnetohydrodynamic squeeze film lubrication with induction effects[50] and plasma porous media MHD generator flow[10], all using NSM. The fundamental advantage of the NSM approach is that it circumvents the traditional requirement of other finite difference schemes for extensive algebraic manipulation and convergence constraints. NSM is based on the classical thermoelectric analogy between thermal and electrical variables. Nevertheless, its capacity to implement in the model any kind of non-linearity (due to boundary conditions, phase-change processes, temperature dependencies of the thermal properties, etc) distinguishes NSM from the analogies generally exposed in text books. A first-order central difference approximation is used for the first derivate and a second-order central difference approximation is used for the second derivate in the dimensionless Eqs. (7) $\sim$ (9). Kirchhoff's law for electrical currents from circuit theory is used to derive the network model and an intimate knowledge of circuit theory is necessary to formulate the problem. Fourier's law of heat conduction is utilized in the spatial discretization of the dimensionless equations. The discretized versions of the dimensionless tangential and axial momentum conservation Eqs. (7) $\sim$ (8) take the form:

$$R_e U_{z,i,j}\frac{U_{\theta,i,j+\Delta Z}-U_{\theta,i,j-\Delta Z}}{\Delta Z}-\frac{U_{\theta,i,j+\Delta Z}+U_{\theta,i,j-\Delta Z}-2U_{\theta,i,j}}{\Delta Z^2}=\frac{U_{\theta,i+\Delta R,j}+U_{\theta,i-\Delta,j}-2U_{\theta,i,j}}{\Delta R^2}$$
$$+\frac{1}{R_{i,j}}\frac{U_{\theta,i+\Delta R,j}-U_{\theta,i-\Delta R,j}}{\Delta R}-(1+Ha^2)\frac{U_{\theta,i,j}}{R_{i,j}^2}-\frac{U_{\theta,i,j}}{Da}-\frac{FsReU_{\theta,i,j}^2}{Da}, \quad (10)$$

$$\frac{U_{Z,i+\Delta R}+U_{Z,i-\Delta R}-2U_{Z,i}}{\Delta R^2}+\frac{1}{R_{i,j}}\frac{U_{Z,i+\Delta R}-U_{Z,i-\Delta R}}{\Delta R}-\frac{Ha^2}{R_{i,j}^2}U_{z,j}-\frac{U_{z,i}}{Da}-\frac{FsReU_{z,j}^2}{Da}=-\alpha. \quad (11)$$

In the Eqs. (10) $\sim$ (11) all the terms can be treated as a current (see Figs. 10 and 11 where the network models are illustrated). Therefore for the discretized tangential momentum Eq. (10) the following currents are defined:

$$\begin{cases} j_{i,j+\Delta Z} = \frac{U_{\theta,i,j+\Delta Z} - U_{\theta,i,j}}{\Delta Z^2} \\ j_{i,j-\Delta Z} = \frac{U_{\theta,i,j} - U_{\theta,i,j-\Delta Z}}{\Delta Z^2} \\ j_{i-\Delta R,j} = \frac{U_{\theta,i,j} - U_{\theta,i-\Delta,j}}{\Delta Z^2} \\ j_{i+\Delta,j} = \frac{U_{\theta,i+\Delta R,j} - U_{\theta,i,j}}{\Delta R^2} \\ j_{i+\Delta,j} = \frac{U_{\theta,i+\Delta,j} - U_{\theta,i,j}}{\Delta R^2} \\ j_{i+\Delta,j} = \frac{U_{\theta,i+\Delta,j} - U_{\theta,i,j}}{\Delta R^2} \\ j_{Z,i,j} = R_e U_{z,i,j} \frac{U_{\theta,i,j+\Delta Z} - U_{\theta,i,j-\Delta Z}}{\Delta Z} \\ j_{Z,i,j} = R_e U_{Z,i,j} \frac{U_{\theta,i,j+\Delta Z} - U_{\theta,i,j-\Delta Z}}{\Delta Z} \\ j_{R,i,j} = \frac{1}{R_{i,j}} \frac{U_{\theta,i+\Delta R,j} - U_{\theta,i-\Delta R,j}}{\Delta R} \\ j_{Da,i,j} = \frac{U_{\theta,i,j}}{Da} + \frac{FsReU^2_{\theta,i,j}}{Da} \\ j_{Ha,i,j} = (1+Ha^2)\frac{U_{\theta,i,j}}{R^2_{i,j}} \end{cases} \tag{12}$$

Similarly for the discretized axial momentum Eq. (11) the following currents are defined:

$$\begin{cases} j_{i-\Delta R} = \frac{U_{Z,i} - U_{Z,i-\Delta R}}{\Delta R^2} \\ j_{i+\Delta} = \frac{U_{Z,i+\Delta R} - U_{Z,i}}{\Delta R^2} \\ j_{Z,i,j} = \alpha \\ j_{R,i} = \frac{1}{R_i} \frac{U_{Z,i+\Delta R} - U_{Z,i-\Delta R}}{\Delta R} \\ j_{Da,i} = \frac{U_{Z,i}}{Da} + \frac{FsReU^2_{Z,i}}{Da} \\ j_{Ha,i} = Ha^2 \frac{U_{Z,i}}{R^2_i} \end{cases} \tag{13}$$

Therefore implementing Kirchhoff's law for electrical currents from circuit theory, the network model is obtained for the entire model:

$$j_{i,j-\Delta Z} + j_{i,j+\Delta Z} + j_{i+\Delta R,j} - j_{i+\Delta R,j} + j_{Z,i,j} + j_{R,i,j} - j_{Da,i,j} = 0, \tag{14}$$

$$j_{i-\Delta R} + j_{i+\Delta R} + j_{\alpha,i} + j_{R,i} - j_{Da,i} - j_{Ha,i} = 0. \tag{15}$$

To introduce the boundary conditions, voltage sources are employed. After experimenting with a few sets of mesh sizes, a region of integration of 200 cells has been selected. The following computations have been performed using NSM to compare with MAPLE F-D solutions. In the NSM computations, the following default values are prescribed: $Ha^2 = 5$, $N = 0.4$, $R_e = 10$ (limit of Darcy law validity), $Da = 1$, $Fs = 1$, $\lambda = 0.5$, $\alpha = 1$. Such values correspond to a highly permeable regime with weak Forchheimer drag effect. We are primarily concerned with the tangential distributions of velocity profiles in the regime. λ is the radius of the inner to outer cylinder, maintained at 0.5 throughout the computations. $\alpha = 1$ corresponds to a constant axial pressure gradient of unity. Validation of the MAPLE solutions has been undertaken with NSM computations; for conservation of space we only present the tangential velocity distributions computed with NSM. In both cases, excellent agreement was obtained with the non-porous solutions of Nath [33]. A particularly important parameter in the computations is Da which represents the permeability of the porous medium. We examine highly porous regimes for which Da will have high values. For the case of infinite permeability, $Da \to \infty$, the model reduces to exactly the equations solved by Nath [33], who used Bessel functions, with the boundary conditions unchanged:

$$\frac{\partial P}{\partial R} = \frac{1}{2}\frac{U^2_\theta}{R}, \tag{16}$$

$$R_e U_z \frac{\partial U_\theta}{\partial Z} - \frac{\partial^2 U_\theta}{\partial Z^2} = \frac{\partial^2 U_\theta}{\partial R^2} + \frac{1}{R}\frac{\partial U_\theta}{\partial R} - (1+Ha^2)\frac{U_\theta}{R^2} - \frac{U_\theta}{Da} - \frac{FsReU^2_\theta}{Da}, \tag{17}$$

$$\frac{\partial^2 U_z}{\partial R^2} + \frac{1}{R}\frac{\partial U_z}{\partial R} - \frac{Ha^2}{R^2}U_z - \frac{U_z}{Da} - \frac{FsReU^2_z}{Da} = -\alpha. \tag{18}$$

Nath [33] demonstrated the symmetry of the solutions about the centre plane of the annulus for the axial velocity profiles; he also highlighted the monotonic nature of solutions from the inner cylinder surface to the outer surface cylinder, for the tangential velocity profiles. These trends are strongly reflected in both sets of MAPLE and NSM computations.

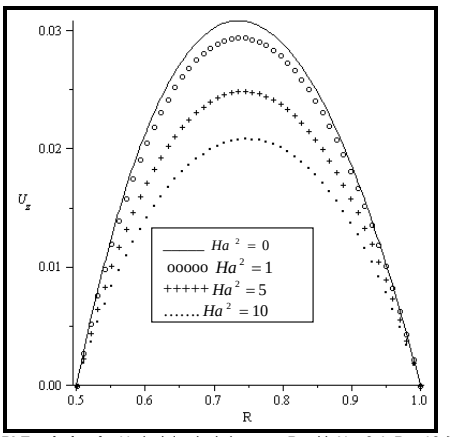

Fig. 4. MAPLE solution for U_Z (axial velocity) versus R with $N = 0.4$, $R_e = 10$ (limit if Darcy law validity), $Da = 1$, $Fs = 1$, $\lambda = 0.5$, $\alpha = 1$, for various squares of the Hartmann number (Ha^2)

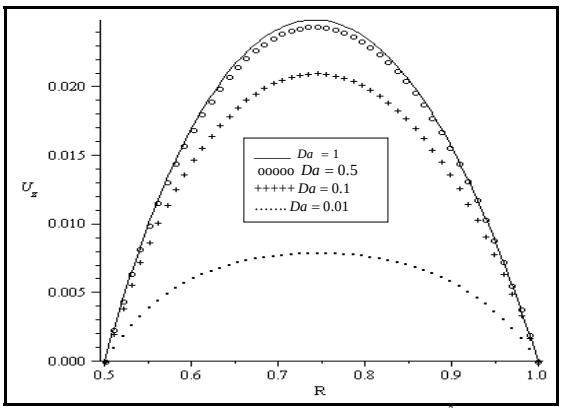

Fig. 5. MAPLE solution for U_Z (axial velocity) versus R with $N = 0.4$, $Ha^2 = 5$, $Re = 10$, $Fs = 1$, $\lambda = 0.5$, $\alpha = 1$, for various Darcy numbers (Da)

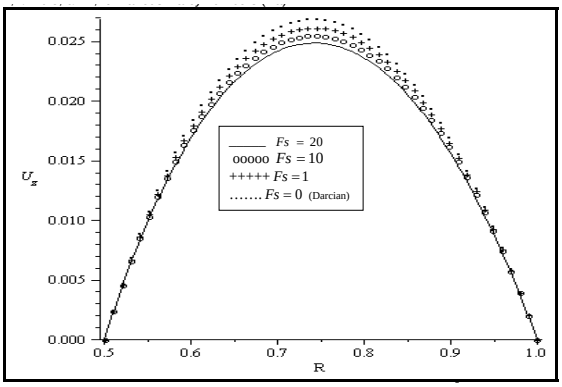

Fig. 6. MAPLE solution for U_Z (axial velocity) versus R with $N = 0.4$, $Ha^2 = 5$, $R_e = 10$, $Da = 1$, $\lambda = 0.5$, $\alpha = 1$, at $Z = 1$ for various Forchheimer numbers (Fs)

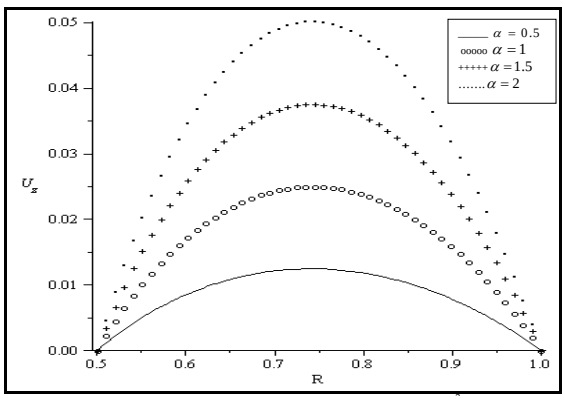

Fig. 7. MAPLE solution for U_Z (axial velocity) versus R with $N = 0.4, Ha^2 = 5, R_e = 10, Da = 1, Fs = 1, \lambda = 0.5$, for various pressure gradient parameter values (α)

5 Results and discussion

In Figs. 4 $\sim$ 7 the axial velocity distributions obtained using the MAPLE finite difference software[1] are presented. As with these and all other distributions, the velocity is plotted along the dimensionless radial coordinate, R. The strong retarding nature of the magneto-hydrodynamic body force on the axial velocity distribution, U_z, in the saturated porous annular regime, is evident in figure 4, where with increasing Ha^2 value, parabolic profiles of axial velocity are strongly decreased across the annulus region. The peak velocity arises at the centre of the annulus i.e. at $R = 0.75$, a pattern which strongly concurs with the analytical solutions of Nath [33], the latter considering both non-conducting $(Ha^2 = 0)$ and electrically-conducting flow $(Ha^2 > 0)$ in the absence of porous drag effects $(Da \to \infty)$. Ha^2 is directly proportional to the characteristic magnetic induction intensity, B_0, and appears in the linear term $-\frac{Ha^2}{R^2}U_z$ arising in the axial momentum balance Eq. (8). As such increasing radial magnetic field, B_o, serves to decelerate axial flow strongly. Such a mechanism can act as a successful inhibiting technique in hydromagnetic materials processing etc, where greater control along the longitudinal axis of the system can be achieved by increasing magnetic field applied in the radial direction (transverse to the Z-axis). The influence of the permeability of the porous medium, as expressed in the Darcy number, Da, on axial velocity is shown in figure 5. The linear porous drag force i.e. Darcian drag force is inversely proportional to Darcy number, as simulated in the term, $-\frac{U_z}{Da}$, also in Eq. (8). An increase in permeability of the annular regime will therefore increase Da which will act to decrease the Darcian drag owing to the progressive depletion of porous medium fibers offering bulk matrix resistance to

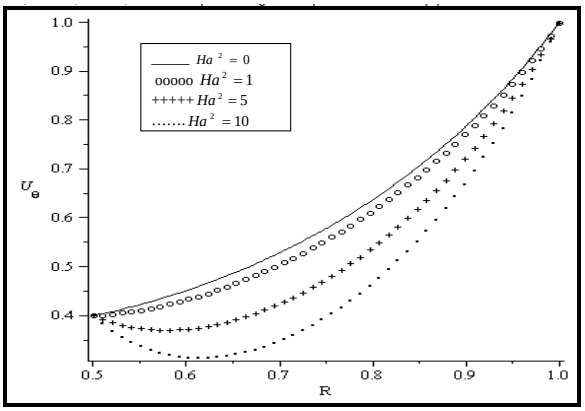

Fig. 8. MAPLE solution for U_θ (tangential velocity) versus R with $N = 0.4, R_e = 10, Da = 1, Fs = 1, \lambda = 0.5, \alpha = 1$, at $Z = 1$ for various squares of the Hartmann number (Ha^2)

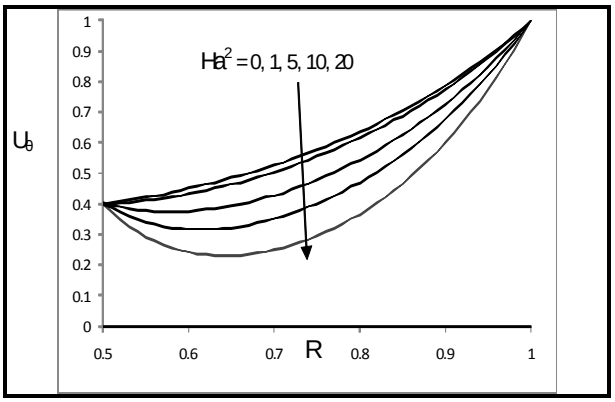

Fig. 9. NSM solution for U_θ (tangential velocity) versus R with $N = 0.4, R_e = 10, Da = 1, Fs = 1, \lambda = 0.5, \alpha = 1$, at $Z = 1$ for various squares of the Hartmann number (Ha^2)

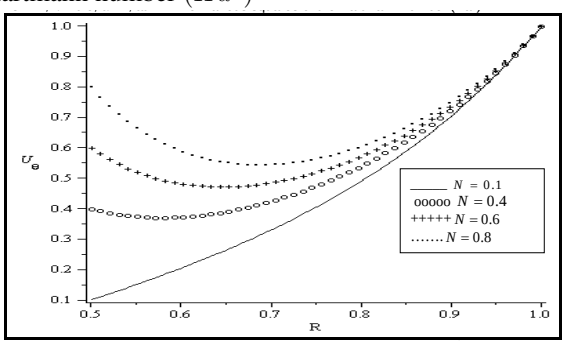

Fig. 10. MAPLE solution for U_θ (tangential velocity) versus R with $Ha^2 = 5, R_e = 10, Da = 1, Fs = 1, \lambda = 0.5, \alpha = 1$, at $Z = 1$ for various relative rotation rate parameters (N)

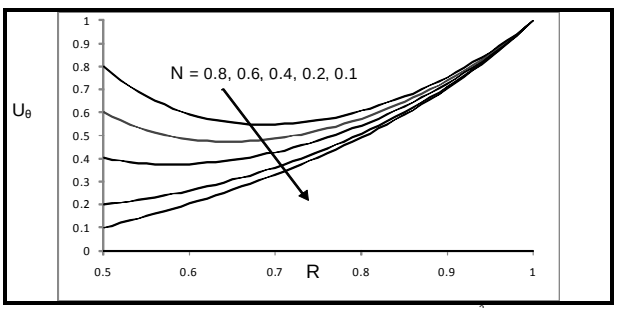

Fig. 11. MAPLE solution for U_θ (tangential velocity) versus R with $Ha^2 = 5, R_e = 10, Da = 1, Fs = 1, \lambda = 0.5, \alpha = 1$, at $Z = 1$ for various relative rotation rate parameters (N)

the flow. Effectively therefore with an increase in Da, axial flow will be accelerated i.e. axial velocity boosted. In agreement with this physical argument, we indeed observe a strong increase in U_Z across the annular zone with a rise in Da from 0.01 (low permeability media) through 0.1, 0.5 to 1.0 (very high permeability media e.g. metallic foams). Again symmetry of the parabolic profiles about the line $R = 0.75$ is evident in Fig. 5. In these and the majority of other profiles $N = 0.4$. N embodies the relative speeds of rotation of the inner to the outer cylinders, $(\frac{\omega_1 a}{\omega_2 b}) = N$ as defined in the second boundary condition of Eq. (9). $N > 0$ implies both cylinders are rotating in the same direction. λ is generally also prescribed as 0.5 so that the outer cylinder radius is twice that of the inner i.e. $b = 2a$ in Fig. 1 and Eq. (5). Effectively then since $N = 0.4$ we have $\omega_2 = 1.25, \omega_1$ i.e. the outer cylinder rotates faster than the inner cylinder. The effect of the second order (quadratic) porous drag on axial velocity is depicted in Fig. 6, as experienced via the Forchheimer number, Fs. A clear impedance is imparted to the axial flow with an increase in Fs from 0 (Darcian case) through 1, 10 to 20. However since the axial velocity magnitudes (U_z) are small, the square of these velocities (U_z^2) will be very small, manifesting in a weak effect of the Forchheimer drag term, $-\frac{FsReU_z^2}{Da}$ in Eq. (8). For constant Reynolds number and Darcy number, the net Forchheimer drag will be of small magnitude in the axial flow explaining the small differences observed in the profiles in Fig. 6. Fig. 7 illustrates the effect of the axial pressure gradient parameter, α, defined in Eq. (5). This parameter appears only in the axial momentum equation as a negative term on the right hand side i.e. transposing to the left this term will become a positive body force and will therefore serve to aid the axial flow (contrary to the Lorentz hydromagnetic drag, axial Darcian drag and axial Forchheimer drag, which are all negative on the left hand side of Eq. (8)). In accordance with this argument, the axial velocity should be boosted considerably with increasing positive values of α; Fig. 7 bears testimony to this logic where we

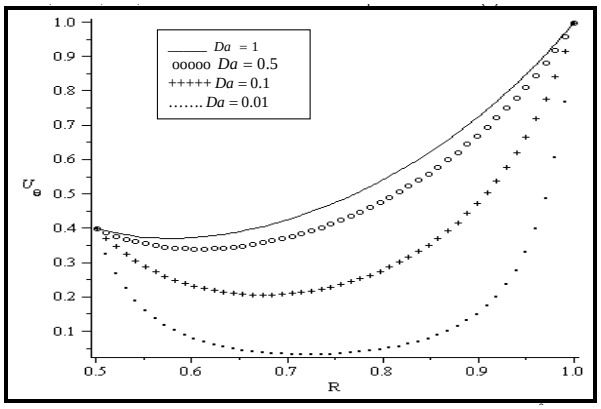

Fig. 12. MAPLE solution for U_θ (tangential velocity) versus R with $Ha^2 = 5, R_e = 10, Da = 1, Fs = 1, \lambda = 0.5, \alpha = 1$, at $Z = 1$ for various relative rotation rate parameters (N)

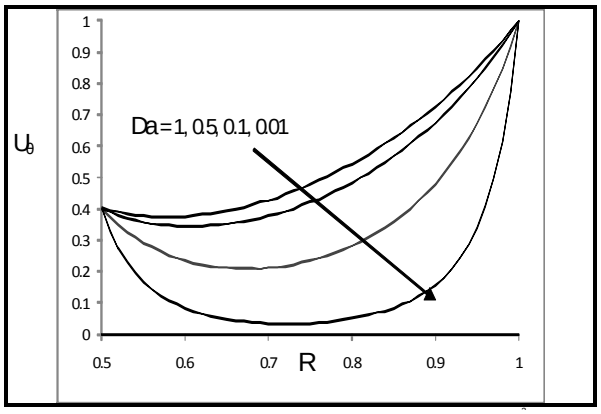

Fig. 13. NSM solution for U_θ (tangential velocity) versus R with $N = 0.4, Ha^2 = 5, R_e = 10, Fs = 1, \lambda = 0.5, \alpha = 1$, at $Z = 1$ for various Darcy numbers (Da)

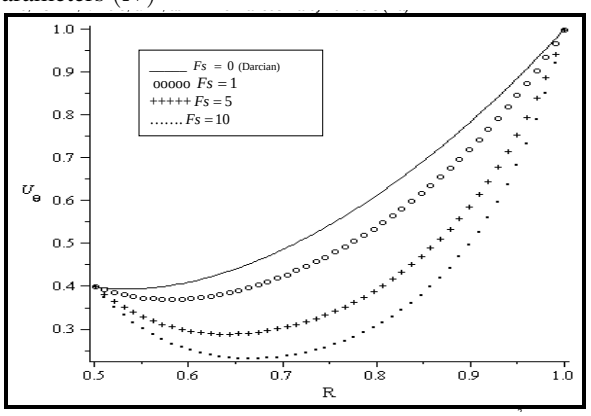

Fig. 14. MAPLE solution for U_θ (tangential velocity) versus R with $N = 0.4, Ha^2 = 5, R_e = 10, Da = 1, \lambda = 0.5, \alpha = 1$, at $Z = 1$ for various Forchheimer numbers (Fs)

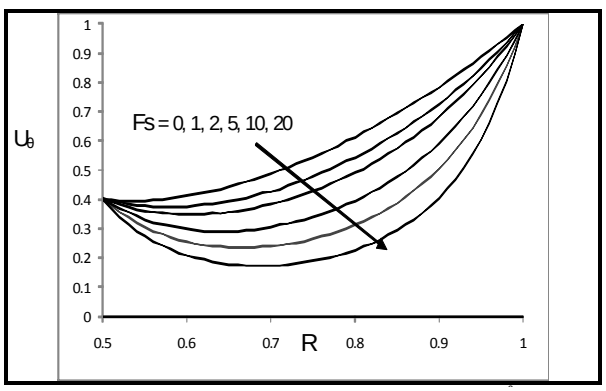

Fig. 15. NSM solution for U_θ (tangential velocity) versus R with $N = 0.4, Ha^2 = 5, R_e = 10, Da = 1, \lambda = 0.5, \alpha = 1$, at $Z = 1$ for various Forchheimer numbers (Fs)

observe a strong elevation in U_z with an increase in α from 0.5 through 1, 2 to 2. As before the profiles sustain a parabolic shape across the entire annular porous medium zone.

We now turn our attention to the tangential velocity evolution in the annular regime. Fig. 8 shows the MAPLE solution for the effect of the square of the Hartmann number on U_θ. The monotonic ascent of the profiles from the inner cylinder wall $(R = 0.5)$ to the outer cylinder wall $(R = 1)$ is evident. Increasing Ha^2 values clearly decelerate the tangential flow. In the tangential momentum Eq. (7), the Lorentz magnetohydrodynamic body force term, $-(1+Ha^2)\frac{U_\theta}{R^2}$ is clearly a retarding term. It will therefore reduce tangential velocity magnitudes throughout the annulus. To validate the MAPLE solutions we have also presented NSM solutions in Fig. 9. Inspection of these figures indicates that the agreement is excellent, which serves to confirm the accuracy of both methods. Indeed both graphs correlate also very well with Nath's solutions [33].

In Figs. 10 and 11, the MAPLE and NSM computed effects of the rotation parameter, N, on U_θ are shown, respectively. In all profiles in both figures, $N < 1$ i.e. the relative rotation rate is low. For $N = 0.5$ (since $\lambda = 0.5$) the cylinders will rotate at the same rate i.e. $\omega_2 = \omega_1 1$. For $N > 0.5$ however the inner cylinder will rotate faster than the outer i.e. $\omega_1 > \omega_2$. As N continues to increase very fast relative rotation is achieved with increasing domination of the inner cylinder i.e. for $N >> 1$, $\omega_1 >> \omega 2$. The axial velocity magnitudes discussed earlier (Figs. 4 $\sim$ 7) are an order of magnitude less than tangential velocity i.e. the tangential flow dominates the annular regime, in consistency with the findings of many other researchers[14]. An increase in N from 0.1, as observed in Fig. 10 (for which $\omega_2 = 5\omega_1$) through 0.4, 0.6 to 0.8 ($\omega_1 = 1.6\omega_2$), substantially increases tangential velocity generally throughout the porous annulus $(R < 0.5 < 1)$, in

particular near the inner cylinder. Further towards the outer cylinder the effect is less dramatic with profiles effectively converging after $R \sim 0.95$. A faster inner cylinder rotation $(\omega_1 > \omega_2)$, is therefore assistive to the tangential flow; the latter is stifled however with greater outer cylinder rotational velocity (i.e. lower N values, for which $(\omega_2 > \omega_1)$. Excellent agreement is seen between the NSM computations (Fig. 11) and the MAPLE computations (Fig. 10) the profiles are practically indistinguishable, confirming the validity of both numerical techniques. Very close correlation to the results of Nath [33] has also been attained, although for brevity the comparisons are omitted here. Neglegible effect on the axial flow was computed for varying N and therefore is excluded from our discussion.

The tangential profiles for various Darcy numbers (Da) obtained with MAPLE and NSM numerical techniques are presented in Figs. 12 and 13, respectively. Almost exactly the same solutions are obtained with an increase in Da from 0.01 (very low permeability annular material) through 0.1, 0.5 to the maximum value of 1 (extremely high permeability) with both computational methods, further validating the present results. As with the axial velocity profile (Fig. 5), increasing Darcy number evidently increases the tangential velocity (however the profiles are monotonic, not parabolic) owing to a simultaneous decrease in tangential Darcian drag force, $-\frac{U_\theta}{Da}$ appearing in Eq. (7). Towards the centerline of the annulus $(R = 0.75)$ tangential velocity is so strongly affected that it almost vanishes i.e. tangential flow is almost eliminated with very low Darcy number $(Da = 0.01)$. Clearly therefore the presence of a porous medium has a strongly inhibiting effect on tangential (and axial) flow and can be implemented as an excellent regulatory mechanism in materials processing, crystal growth, magnetic energy systems etc.

Finally in Figs. 14 and 15 the effect of the Forchheimer number, Fs, on tangential velocity development in the annulus is shown. Correlation between the MAPLE and NSM solutions is again excellent. As with the axial flow, tangential Forchheimer drag, $-\frac{FsReU_\theta^2}{Da}$ has an impeding effect on the tangential flow. A rise in Fs from 0 (Darcian case) through 1, 5 to 10 (strong second order drag) considerably inhibits the tangential flow. The effect is substantially greater than for the axial flow, as indicated by the large differences in the profiles. Forchheimer drag therefore serves to control the tangential flow to a much greater degree than the axial flow and may be exploited thereof, for example, in chemical engineering processing.

6 Conclusion

Hydromagnetic flow in a non-Darcian porous medium annular space confined between two coaxial rotating cylinders in the presence of a radial magnetic field, has been studied. MAPLE finite difference and NSM computational methods have been discussed for solving the transformed conservation equations. Excellent agreement has been obtained. The solutions have shown that with increasing magnetic field intensity (corresponding to an increase in Hartmann number (Ha)), and increasing inertial porous media drag (corresponding to a rise in Forchheimer number (Fs)), both axial and tangential flow are retarded although to significantly different extents. An increase in permeability of the regime (as simulated via an increase in Darcy number (Da)) and a rise in pressure gradient parameter (α) however both accelerate the axial flow. An increase in Darcy number (Da) also boosts the tangential flow field. Increasing relative rotation parameter (N) also significantly accelerates the tangential flow especially at the inner cylinder boundary of the porous medium annulus. The current study has examined isotropic porous media. Future communications will describe anisotropic porous media effects and also include magnetic induction effects. Applications of the present model arise in MHD energy systems, controlled crystal growth technologies, chemical engineering, astrophysical flows and magneto-metallurgical flow processing.

References

[1] Maplesoft. A division of Waterloo Maple Incooporation, 2011, Http://maplesoft.com/products/maple/technical.aspx.
[2] Microsim P. 6.0. *Irvine, California 92718*. Microsim Corporation, 1994. 20 Fairbanks.
[3] K. Arora, P. Gupta. Magnetohydrodynamic flow between two rotating coaxial cylinders under radial magnetic field. *Physics of Fluids*, 1972, **15**(6): 1146–1148.
[4] J. Bear. *Dynamics of Fluids in Porous Media*. Dover, New York, 1988.

[5] O. Bég, R. Bhargava, et al. Computational modeling of biomagnetic micropolar blood flow and heat transfer in a two-dimensional non-darcian porous medium. *Meccanica Journal*, 2008, **43**: 391–410.

[6] O. Bég, H. Takhar, et al. Numerical study of heat transfer of a third grade viscoelastic fluid in non-darcy porous media with thermophysical effects. **in:** *Physica Scripta: Proceedings of Royal Swedish Academy of Sciences*, 2008, **77**: 1–11.

[7] O. Bég, H. Takhar, A. Singh. Multiparameter perturbation analysis of unsteady oscillatory magnetoconvection in porous media with heat source effects. *International Journal of Fluid Mechanics Research*, 2005, **32**(6): 635–661.

[8] O. Bég, J. Zueco, et al. Magneto-hydrodynamic natural convection flow from a sphere to a non-darcian porous medium with heat generation or absorption effects: network simulation. *International Journal of Thermal Sciences*, 2009, **48**: 913–921.

[9] O. Bég, J. Zueco, H. Takhar. Laminar free convection from a continuously-moving vertical surface in thermally-stratified non-darcian high-porosity medium-network numerical study. *International Communications in Heat and Mass Transfer*, 2008, **35**: 810–816.

[10] O. Bég, J. Zueco, H. Takhar. Unsteady magnetohydrodynamic hartmann-couette flow and heat transfer in a darcian channel with hall current, ionslip, viscous and joule heating effects: Network numerical solutions. *Communications in Nonlinear Science and Numerical Simulation*, 2009, **14**(4): 1082–1097.

[11] R. Bhargava, H. Rawat, et al. Pulsatile magneto-biofluid flow and mass transfer in a non-darcian porous medium channel. *Mecannica Journal*, 2007, **42**: 247–262.

[12] R. Bhargava, H. Takhar, et al. Finite element solutions for non-newtonian pulsatile flow in a non-darcian porous medium conduit. *Non-Linear Analysis: Modeling and Control Journal*, 2007, **12**(3): 317–327.

[13] A. Chamkha. MHD-free convection from a vertical plate embedded in a thermally stratified porous medium with hall effects. *Applied Mathematical Modelling*, 1997, **21**(10): 603–609.

[14] S. Chandrasekhar. *Hydromagnetic and Hydrodynamic Stability*. Clarendon Press, Oxford, 1961.

[15] L. Debnath. Inertial oscillations and hydromagnetic multiple boundary layers in a rotating fluid. *Journal of Applied Mathematics and Mechanics / Zeitschrift fr Angewandte Mathematik und Mechanik*, 1975, **55**: 141–150.

[16] L. Debnath, S. Roy, A. Chatterjee. Effects of hall current on unsteady hydromagnetic flow past a porous plate in a rotating fluid system. *Journal of Applied Mathematics and Mechanics / Zeitschrift fr Angewandte Mathematik und Mechanik*, 1979, **59**: 469.

[17] A. Dybbs, R. Edwards. A new look at porous media fluid mechanics - darcy to turbulent. *Fundamentals of Transport Phenomena in Porous Media*, 1984, 201–256. NATO Applied Sciences Series.

[18] C. Geindreau, J. Auriault. Magnetohydrodynamic flows in porous media. *Journal of Fluid Mechanics*, 2002, **466**: 343–363.

[19] B. Ghosh, N. Ghosh. Mhd flow of a visco-elastic fluid through porous medium. *International Journal of Numerical Methods Heat Fluid Flow*, 2001, **11**(7): 682–698.

[20] R. Gulab, R. Mishra. Unsteady flow through magneto—hydrodynamic porous media. *Indian Journal of Pure and Applied Mathematics*, 1977, **8**: 637–42.

[21] A. Hamza. The magnetohydrodynamic effects on a fluid film squeezed between two rotating surfaces. *Journal of Physics D: Applied Physics*, 1991, **24**: 547–554.

[22] T. Hayat, M. Husain, M. Khan. Effects of hall current on f lows of a burgers fluid through a porous medium. *Transport in Porous Media*, 2007, **68**(2): 249–263.

[23] T. Hayat, M. Javed, N. Ali. MHD peristaltic transport of a jeffery fluid in a channel with compliant walls and porous space. *Transport in Porous Media*, 2008, **74**(3): 259–274.

[24] W. Hughes, R. Elco. Magnetohydrodynamic lubrication flow between parallel rotating disks. *The Journal of Fluid Mechanics*, 1962, **13**: 21–32.

[25] T. Katukani. Hydromagnetic flow due to a rotating disk. *Journal of the Physical Society of Japan*, 1962, **17**: 1496–1506.

[26] M. Khan, Z. Abbas, T. Hayat. Analytic solution for flow of sisko fluid through a porous medium. *Transport in Porous Media*, 2008, **71**(1): 23–37.

[27] V. Kumar. Steady laminar hydromagnetic flow in the annular region between two coaxial rotating circular cylinders with an impressed radial magnetic field. *University of Roorkee Research Journal*, 1966, **9**(1-2): 9–15.

[28] N. Leeorin, I. Rogachevskii, et al. Axisymmetric flow between differentially rotating spheres in a dipole magnetic field. *Journal of Fluid Mechanics*, 1997, **344**(1): 213–244.

[29] S. Lin. Laminar hydromagnetic flow between concentric rotating cylinders. *Physics Fluids (Research Notes)*, 1970, **43**(7): 1873–74.

[30] J. Mahapatra. A note on the unsteady motion of a viscous conducting liquid between two porous concentric circular cylinders acted on by a radial magnetic field. *Applied Scientific Research*, 1973, **27**(1): 274–282.

[31] S. Meena, P. Kandaswamy. The hydromagnetic flow between two rotating eccentric cylinders. *International Journal of Fluid Mechanics Research*, 2002, **29**: 40–57.

[32] N. Murthy, J. Feyen. Influence of variable permeability on the dispersion of a chemically reacting solute in porous media. *International Journal of Engineering Science*, 1989, **27**(12): 1661–1671.

[33] G. Nath. Tangential velocity profile for axial flow through two concentric rotating cylinders with radial magnetic field. *Defence Science Journal*, 1970, **20**(4): 207–212.

[34] L. Pop. On the hydromagnetic flow due to an impulsive rotating disk. *Journal of Applied Mathematics and Mechanics / Zeitschrift fr Angewandte Mathematik und Mechanik*, 1974, **54**(4): 284–286.

[35] V. Prasad, V. Rao. Hydromagnetic flow between two parallel porous walls in a rotating system. *Defence Science Journal*, 1978, **28**: 51–58.

[36] V. Prasad, H. Takhar, et al. Numerical study of hydromagnetic viscous plasma flow with hall current effects in rotating porous media. **in:** *Invited paper, 53rd Congress ISTAM*, University College of Engineering, Osmania University, Hyderabad, India, 2008, 147–157.

[37] S. Rawat, R. Bhargava, O. Bég. A finite element study of transport phenomena in mhd micropolar flow in a darcy-forchheimer porous medium. **in:** *WCECS International Conference of Chemical Engineering*, San Francisco, California, USA, 2007, 169–174.

[38] V. Sastry, K. Rao. Hydromagnetic stokes flow past a rotating sphere. *The Journal of Fluid Mechanics*, 1978, **88**: 757–768.

[39] P. Sengupta, S. Ghosh. Steady hydromagnetic flow between two porous concentric circular cylinders. *Czechoslovak Journal of Physics*, 1975, **25**(5): 514–520.

[40] G. Seth, S. Ghosh. Unsteady hydromagnetic flow in a rotating channel in the presence of inclined magnetic field. *International Journal of the Engineering Science*, 1986, **24**(7): 1183–1193.

[41] G. Seth, R. Jana, M. Maiti. Unsteady hydromagnetic couette flow in a rotating system. *International Journal of the Engineering Science*, 19982, **20**(9): 989–999.

[42] B. Sharma, A. Jha, R. Chaudhary. MHD forced flow of a conducting viscous fluid through a porous medium induced by an impervious rotating disk. *Romanian Journal of Physics*, 2007, **52**(1-2): 73–84.

[43] S. Singh, H. Takhar, P. Ram. Magnetohydrodynamic flow between coaxial rotating cone and a cylinder under the influence of radial a mgnetic field. *Journal of the Magnetohydrodynamics and Plasma Research*, 1996, **2**: 21–32.

[44] C. Stephenson. Magnetohydrodynamic flow between rotating coaxial disks. *Journal of the Fluid Mechanics*, 1969, **38**: 335–352.

[45] H. Takhar, O. Bég. Effects of transverse magnetic field, prandtl number and reynolds number on non-darcy mixed convective flow of an incompressible viscous fluid past a porous vertical flat plate in saturated porous media. *International Journal of Energy Research*, 1997, **21**: 87–100.

[46] H. Takhar, R. Bhargava, et al. Finite element modeling of laminar flow of a third grade fluid in a darcy-forchheimer porous medium with suction effects. *International Journal of Applied Mechanics Engineering*, 2007, **12**(1): 215–233.

[47] M. Tawil, M. Kamel. MHD flow under stochastic porous media. *Energy Conversion Management*, 1994, **35**(11): 991–997.

[48] V. Vidyanidhi, V. Rao. Hydromagnetic flow in a rotating straight pipe. *Journal of the Physical Society of Japan*, 1969, **27**(3): 799–800.

[49] J. Zueco, F. Alhama. Simultaneous inverse determination of the temperature-dependent thermophysical properties of fluids using the network simulation method. *International Journal of Heat and Mass Transfer*, 2007, **50**: 3234–3243.

[50] J. Zueco, O. Bég. Network numerical analysis of hydromagnetic squeeze film flow dynamics between two parallel rotating disks with induced magnetic field effects. *Tribology International*, 2010, **43**: 532–543.